ACS APPLIED MATERIALS & INTERFACES

Research Article

Cite This: ACS Appl. Mater. Interfaces 2019, 11, 4809−4819

www.acsami.org

Protection of Nanostructures-Integrated Microneedle Biosensor Using Dissolvable Polymer Coating

Fanmao Liu,[†,‡,⊥] Zhihong Lin,[‡,⊥] Quanchang Jin,[‡] Qianni Wu,[‡,§] Chengduan Yang,[†] Hui-Jiuan Chen,[‡] Zihan Cao,[‡] Di-an Lin,[‡] Lingfei Zhou,[‡] Tian Hang,[‡] Gen He,[‡] Yonghang Xu,[∥] Wenhao Xia,[†] Jun Tao,*[,†] and Xi Xie*[,†,‡]

[†]Department of Hypertension and Vascular Disease, The First Affiliated Hospital, Sun Yat-sen University, 510080 Guangzhou, China

[‡]State Key Laboratory of Optoelectronic Materials and Technologies, School of Electronics and Information Technology, Sun Yat-sen University, 510006 Guangzhou, China

[§]State Key Laboratory of Ophthalmology, Zhongshan Ophthalmic Center, Sun Yat-sen University, 510060 Guangzhou, China

[∥]School of Materials Science and Energy Engineering, Foshan University, 528000 Foshan, China

S *Supporting Information*

ABSTRACT: Real-time transdermal biosensing provides a direct route to quantify biomarkers or physiological signals of local tissues. Although microneedles (MNs) present a mini-invasive transdermal technique, integration of MNs with advanced nanostructures to enhance sensing functionalities has rarely been achieved. This is largely due to the fact that nanostructures present on MNs surface could be easily destructed due to friction during skin insertion. In this work, we reported a dissolvable polymer-coating technique to protect nanostructures-integrated MNs from mechanical destruction during MNs insertion. After penetration into the skin, the polymer could readily dissolve by interstitial fluids so that the superficial nanostructures on MNs could be re-exposed for sensing purpose. To demonstrate this technique, metallic and resin MNs decorated with vertical ZnO nanowires (vNWs) were employed as an example. Dissolvable poly(vinyl pyrrolidone) was spray-coated on the vNW-MNs surface as a protective layer, which effectively protected the superficial ZnO NWs when MNs penetrated the skin. Transdermal biosensing of H_2O_2 biomarker in skin tissue using the polymer-protecting MNs sensor was demonstrated both ex vivo and in vivo. The results indicated that polymer coating successfully preserved the sensing functionalities of the MNs sensor after inserting into the skin, whereas the sensitivity of the MN sensor without a coating protection was significantly compromised by 3-folds. This work provided unique opportunities of protecting functional nanomodulus on MNs surface for minimally invasive transdermal biosensing.

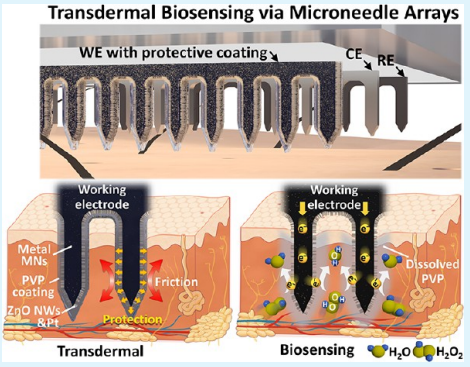

KEYWORDS: *microneedle, biosensing, nanostructure, dissolvable polymer coating, transdermal biosensing*

INTRODUCTION

Detection of biomarkers in biological samples or biofluidics could provide important indications of health or disease states. For example, signaling molecule, H_2O_2, is involved in many biological processes and works as an important biomarker in DNA damage, protein synthesis, cell apoptosis, etc.;[1,2] NO biomarker is a free radical in human body, but an over-production of NO might indicate cancer progression;[3−5] blood glucose concentration directly indicates the insulin level of patients affected by diabetes mellitus; dopamine functions as a neurotransmitter that plays important roles in cognition, learning, and fluctuations in mental state.[6] Benefiting from the emerging nanoscience and nanotechnology, we have recently made significant progress in biosensing, ranging from advanced electrochemical biodevices,[7] field-effect transistor biodevices,[8] microfluidic devices,[9] etc. Compared to conventional sensors, biosensors based on nanostructural materials possess more appealing advantages, e.g., high sensitivity, large specific surface area, high electron mobility, and easy to be decorated or modified for multifunctional applications, etc.[10−13] For instance, biosensors based on Au nanoparticles-decorated graphene framework could achieve 1 μM sensitivity of H_2O_2 detection;[14] picomolar-scale limit of detection of NO was obtained via porphyrin-functionalized graphene field-effect transistor.[15]

Most of the existing nanomaterials-integrated biodevices functioned in vitro or ex vivo by detecting target molecules in a solution, requiring collection of phosphate-buffered saline (PBS) solution or extraction of biofluids such as blood, sweat, or urine from body and to be placed on a sensor.[16−18] However, in vitro or ex vivo biosensing lacks the capability to real-time and

Received: October 30, 2018
Accepted: January 10, 2019
Published: January 10, 2019

Downloaded via MIAMI UNIV on October 21, 2019 at 15:56:45 (UTC).
See https://pubs.acs.org/sharingguidelines for options on how to legitimately share published articles.

© 2019 American Chemical Society

DOI: 10.1021/acsami.8b18981
ACS Appl. Mater. Interfaces 2019, 11, 4809−4819

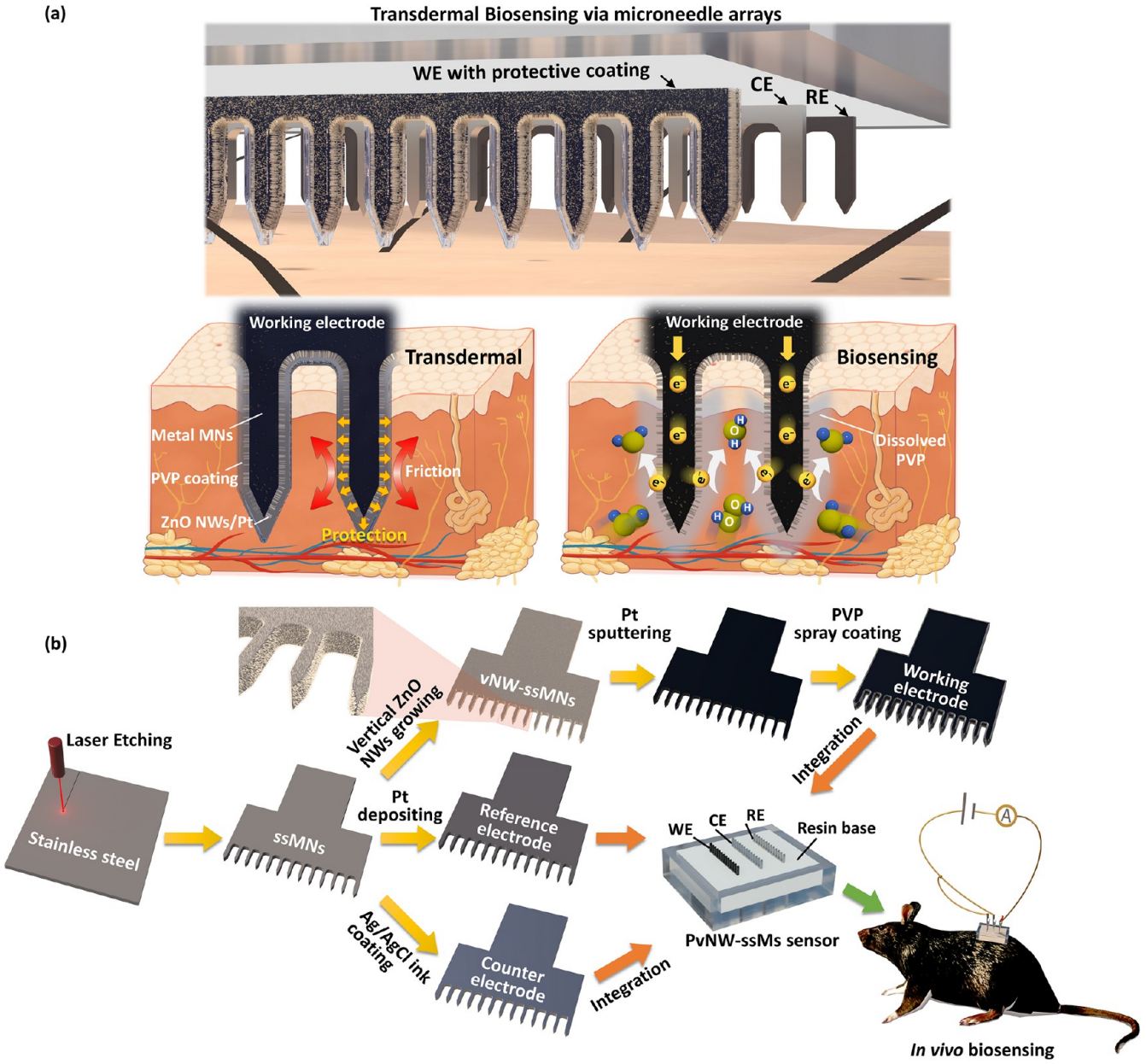

Figure 1. (a) Schematics of PvNW-ssMNs electrochemical sensor for subcutaneous H_2O_2 monitoring. Three electrodes based on ssMNs were integrated into a biosensor for painless transdermal. ZnO NWs/Pt nanostructures were fabricated superficially on the ssMNs with dissolvable PVP layer coating, forming the working electrode (WE). PVP coating protected ZnO NWs from mechanical damage due to the friction from the skin tissue and then rapidly dissolved in interstitial fluid, exposing ZnO NWs/Pt to subcutaneous H_2O_2 sensing. (b) Fabrication process of PvNW-ssMNs electrochemical sensor. ssMNs were first fabricated by laser micromachining as the bases of electrodes. ZnO NWs were hydrothermally synthesized on the MNs surface, later sputtered with a thin layer of Pt. PVP layer was spray coated on vNW-ssMNs to complete the fabrication of PvNW-ssMNs (WE). The sensor was completed via assembling the WE, Pt deposited reference electrode (RE) and Ag/AgCl ink painted counter electrode (CE).

continuous monitoring of the local tissue in situ. On the other hand, conventional in vivo sensing or transdermal sensing was generally performed by sticking metallic needle tubing penetrating through the skin into vessels and inner tissues.[11,19] However, these techniques are invasive to induce potential lesions and undesirable wounds or even infections. The development of nanomaterial-based biosensor for noninvasive or minimally invasive sensing in vivo is still in demand.

Microneedles (MNs) as an emerging technology for transdermal applications have achieved great success both on drug delivery[20−25] and biosensing[3,26,27] due to the simple, painless, and minimally invasive nature of MNs as transdermal tools. For example, Sullivan et al. applied microneedle vaccination to achieve efficient lung virus clearance and enhanced cellular recall responses;[28] Xie et al. successfully developed dissolvable microneedles for effective analgesia on local neuropathic pain.[29] Application of MNs to detect biomarkers in vivo by penetrating skin or endothelium has attracted great research interest, whereas recent research was mainly based on monostructure MNs as electrodes without the integration of nanostructural materials to improve the sensing performance or enhance the sensing functionalities.[30,31] The strategy of integrating MNs with nanostructural materials on the MNs surface for enhanced transdermal biosensing is rarely reported

DOI: 10.1021/acsami.8b18981
ACS Appl. Mater. Interfaces 2019, 11, 4809−4819

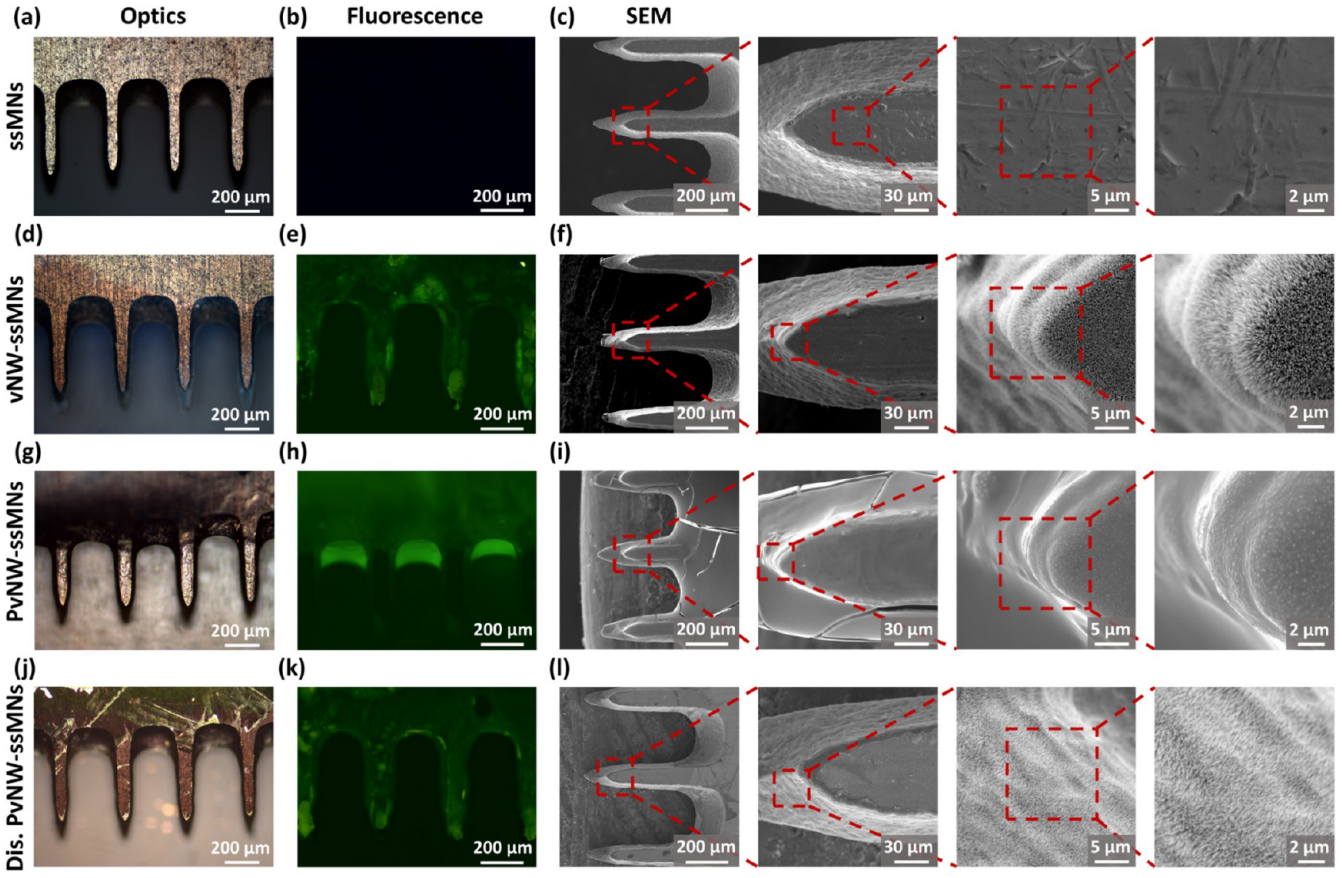

Figure 2. Characterization of the nanostructures and coating on stainless steel MNs. Microscopic images of (a–c) as-fabricated ssMNs, (d–f) vertical ZnO NWs grown on ssMNs, (g–i) PVP spray-coated vNW-ssMNs, and (j–l) PvNW-ssMNs with PVP coating dissolved. Microscopic images from left to right in each panel: optical microscopy, fluorescence microscopy, and SEM images at four magnifications, respectively.

so far due to the difficulties that the superficial nanostructures were likely to be easily damaged by mechanical compression and friction from skin tissues during the MNs insertion process.

In this work, we developed an engineered strategy of applying dissolvable polymer coating to protect nanostructures-integrated MNs from mechanical destruction during MNs transdermal process (Figure 1a). The polymer coating protected the superficial nanostructures from destructive compression and friction when MNs were inserted into the skin, and then rapidly dissolved in interstitial fluid of the dermis and exposed MNs surface for sensing applications. Vertical ZnO nanowires (ZnO NWs) were fabricated on stainless steel MNs (ssMNs) surface as representative nanostructure for demonstration. Dissolvable poly(vinyl pyrrolidone) (PVP) were coated on the vNW-MNs surface as a protective layer via a spray-coating process, and the effectiveness of protection was investigated by morphological examination of superficial ZnO NWs before and after ssMNs penetrated the skin. Similar investigation on resin MNs (rMNs) with ZnO NWs integrated was also carried out for verifying the protecting effectiveness of PVP coating on different materials. In addition, ex vivo and in vivo transdermal electrochemical sensing of the H_2O_2 biomarker in dermis using the PVP-protected vNW-ssMNs (PvNW-ssMNs) as the working electrode (WE) was demonstrated, indicating the intact sensing functionalities of vNW-ssMNs after being inserted into the skin. This work provided a unique solution to protect functional nanomodulus on MNs surface during the skin penetration process, and might open new opportunities for integration of various nanostructures with MNs for minimally invasive transdermal biosensing.

EXPERIMENTAL SECTION

Fabrication of Stainless Steel Microneedles (ssMNs) and Resin Microneedles (rMNs). The ssMNs were etched from 200 μm thick 316L stainless steel plates by laser microetching. The design is shown in the Supporting Information Figure S1. The rMNs were obtained via a micromolding process, described in detail in the Supporting Information Note 3 and Figure S3.

Synthesis of Vertical ZnO Nanowires (ZnO NWs). Vertical ZnO NWs on the surface of ssMNs and rMNs were synthesized by the hydrothermal growth approach. First, 20 nm thick ZnO was sputtered on ssMNs (rMNs) as the seed layer via radio frequency (RF) magnetron sputtering. Then, the seeded ssMNs (rMNs) were immersed into aqueous solutions containing 25 mM zinc nitrate hydrate [$Zn(NO_3)_2{\cdot}6H_2O$] and 25 mM hexamethylenetetramine ($C_6H_{12}N_4$) at 90 °C for 3 h, when the microneedles were oriented with tips pointed downward. Afterward, the microneedles were rinsed in deionized water (DI) water to remove byproducts on the surface and then dried in ambient.

Spray-Coating PVP Protective Layer. Ethanol solutions, 20 wt % PVP (average molecular weight ~360k, Sigma #V900010), were prepared. A spraying gun with a 0.4 mm diameter nozzle was used to generate spray droplets of sub-millimeter diameter, and the homogeneity of the coating was enhanced by mounting MNs samples on a 10 rpm rate rotating stage. High-purity nitrogen was used as the working gas for spray with 0.1 MPa output pressure. The spraying process lasted for 30 s, then the samples were dried and preserved in a vacuum dryer.

DOI: 10.1021/acsami.8b18981
ACS Appl. Mater. Interfaces 2019, 11, 4809–4819

Examination of Protective Effect of PVP Coating. The robustness of PvNW-ssMNs was examined in two ways. One was to compared the morphological changes of ZnO NWs before and after penetrating PvNW-ssMNs into a piece of pigskin. Another approach was to keep PvNW-ssMNs inserted in the pigskin and burn them together at 800 °C in the furnace for 30 min, completely wiping out the PVP coating and the adhering skin tissues but retaining the ZnO NWs. The protection results of the PVP-coated ZnO NWs on rMNs was only examined by the first method described above due to the low melting point of the resin materials.

In Vitro Electrochemical Analysis of Pt-Sputtered vNW-ssMNs Electrode. A standard three-electrode electrochemical workstation (CH Instrument, 700E) was used to examine the electrochemical property of Pt-sputtered vNW-ssMNs electrodes. The electrode was connected as the working electrode, coupled with a commercial Pt counter electrode and a Ag/AgCl reference electrode. The electrochemical activities of the MNs were evaluated via both cyclic voltammetry (CV) and amperometric $I-t$ curve. The sensitivity was calculated from the amperometric response via linear regression.

Construction of PvNW-ssMNs Electrochemical Sensor. The PvNW-ssMNs were used as the working electrode in the three-electrode electrochemical sensor. A layer of Pt with the thickness <20 nm was sputtered on ZnO NWs before PVP coating, working as the sensing receptor that catalytically decomposes H_2O_2 to general electrochemical signals. Counter electrode and reference electrode were also fabricated based on ssMNs for transdermal application. Bared ssMNs were deposited with inner 100 nm Ti and external 300 nm Pt by RF sputtering to form the counter electrode, and another one was painted with Ag/AgCl ink (ALS Co., Ltd) to obtain the reference electrode. Three electrodes were mounted in a three-dimensional-printed clear resin case ($10 \times 12 \times 2.7$ mm^3, wall thickness of 1 mm) with the handles penetrating the seams on the bottom, separated from each other by 2 mm. The electrodes and the case were then fixed and insulated via light-curing resin (color white), leaving only the tips of the ssMNs exposed. The PvNW-ssMNs sensor was finally obtained via electrically wiring by clamping mini-alligator clips on the handles of three electrodes.

Ex Vivo Test of PvNW-ssMNs Sensor on Pigskin Model. Prior to the MNs insertion, 75% alcohol was used to wash and disinfect the pigskins ($15 \times 15 \times 3$ mm^3), which were immersed and soaked in PBS solution containing different concentrations of H_2O_2 (0, 0.1, 0.2, 0.5, and 1 M) at 4 °C for 24 h, allowing H_2O_2 to diffuse into the skin tissue to saturation. PvNW-ssMNs sensor was pressed against the pigskin and the electrical current signals were recorded under applied potential of −1 V. To determine the actual H_2O_2 concentration in soaked pigskins, the skin tissues were minced and quantitatively analyzed by the H_2O_2 assay kit, see the Supporting Information for details.

In Vivo Test of PvNW-ssMNs Sensor on Mice Model. Animal studies were approved by the Sun Yat-sen University Institutional Animal Care and Use Committee. All animals received humane care in compliance with institutional guidelines. C57BL/6 mice were obtained and experimentally studied both at the Animal Facility of Sun Yat-sen University. The mice were anesthetized and skin prepared at the dorsum. Each sensor was applied at the dorsum and electrochemical signal under −1 V potential was recorded 5 min after the application to guarantee the complete dissolving of PVP coating. At the indicated time point, 0.3 mL 1 mM H_2O_2 PBS solution was subcutaneously injected at two injection points successively as described in the Results and Discussion section.

Biocompatibility and Biosafety Tests of PvNW-ssMNs Sensor Application. Local skin irritation caused by sensor application was tested. The PvNW-ssMNs sensor was pressed against the back of the mice and electric bias of −1 V was applied for 2000 s. The mouse was returned to cage for 12 h after the sensor application and removal, then the sensor-treated local skin tissue was dissected, fixed, and stained with hematoxylin and eosin (H&E) for optical microscopic (OM) observation.

RESULTS AND DISCUSSION

The schematics of the ssMNs fabrication and coating procedure are illustrated in Figure 1b. The surface morphology of ssMNs at each fabrication step was characterized with optical microscopy, scanning electron microscopy (SEM), and fluorescence microscopy (FM), as the decoration of ZnO material would produce photoluminescence that is excited by UV light.[32] All micrographs are listed in Figure 2. In the first step, the ssMNs were prepared using direct laser microetching on a planar stainless steel substrate. This produced planar MNs patch with sharp needle tips. The diameter of each tip is ∼200 nm, the length is 680 μm, and the distance between each tip is 250 μm. See Figure S1 in the Supporting Information for the detailed design of the ssMNs. Morphologies of the as-fabricated ssMNs are shown in Figure 2a−c, only scratches and pits on the surface can be observed and no fluorescence signal could be detected (Figure 2b) with UV exciting light (330−380 nm). In the second step, 20 nm thick ZnO layer was deposited on the ssMNs surface through RF magnetron sputtering, which served as the seed layer for the hydrothermal growth of ZnO NWs. The ssMNs patch was incubated in aqueous solutions containing 25 mM $Zn(NO_3)_2$ and 25 mM hexamethylenetetramine at 90 °C for 3 h, which produced vertical ZnO NWs that conformally and densely covered each tip, as presented in Figure 2f. The vertical ZnO NWs were ∼100 nm in diameter and 1−2 μm in length. When excited by UV light, the vNW-ssMNs emitted green fluorescence corresponding to intrinsic-defects-induced photoluminescence emission of ZnO nanostructures at 510 nm (Figure 2e),[33] confirming the successful decoration of ZnO NWs. The inhomogeneous green fluorescence observed in Figure 2e can be attributed to incidental ZnO nanostructures assembled during the growth process of ZnO NWs. To protect the surface of ZnO NWs, water-soluble PVP was coated on the vNW-ssMNs surface via spraying 20 wt % PVP ethanol solution. PVP was employed as the coating material due to its excellent biocompatibility and water solubility.[34] Other types of water-soluble and biocompatible polymers, such as polysaccharide (carboxymethyl cellulose, chitosan, sodium alginate), hyaluronic acid, etc., or various polymerization degrees of PVP, could be also applied as protection coating for MNs. The choice of PVP as the coating material in this work was mainly targeted by choosing the appropriate polymer material with a rapid water-dissolving rate and good biosafety records. The superficial ZnO NWs on each tip were completely embedded by a thick layer (2−5 μm) of PVP, as observed via SEM (Figure 2i). In Figure 2h, the green fluorescence became stronger after the PVP coating, attributed to the passivation of surface defects on ZnO NWs that were caused by the PVP capping.[35] When PvNW-ssMNs were immersed in DI water for 2 min at room temperature, the PVP coating rapidly dissolved and the superficial ZnO NWs were exposed again. Intact ZnO NWs were observed to stand vertically on the tip in a profile similar to that of the ZnO NWs prior to PVP coating, as shown in Figure 2l, indicating that spray-coating was nondestructive to the high-aspect-ratio nanotopography on the surface. Further proof is from Figure 2k, where green fluorescence recovered to similar intensity as that in Figure 2e. Meanwhile, PVP residue was rarely observed on the MNs surface, suggesting the PVP was highly dissolvable in water, allowing the embedded nanostructure to be re-exposed on the surface.

The capability of PVP coating to protect superficial ZnO vNWs after insertion into pigskin was examined ex vivo. First, to

DOI: 10.1021/acsami.8b18981
ACS Appl. Mater. Interfaces 2019, 11, 4809−4819

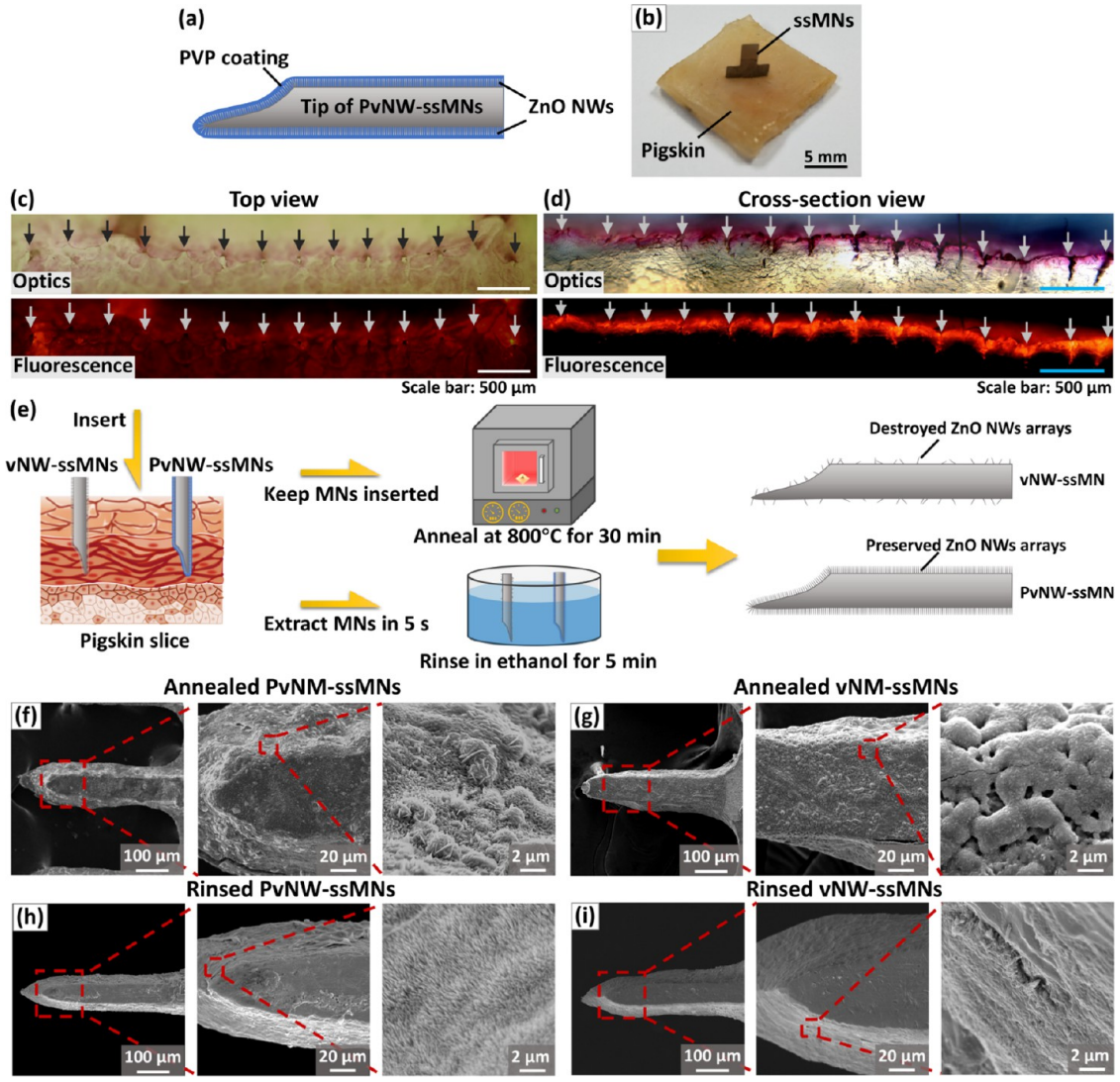

Figure 3. Protective effect of PVP coating on vNW-ssMNs during transdermal process. (a) Schematic of the structure of the PvNW-ssMNs tip. (b) Photographic image of the ssMNs' insertion into pigskin. (c, d) Top and cross-sectional views of the micrographs of skin tissue after ssMNs penetration, respectively. Tips of ssMNs were stained with a red fluorescent dye, rhodamine B, for exhibiting tip-holes in both OM (top panels) and FM (bottom panels) observations. Arrows indicated the ssMNs insertion sites. (e) Schematics of the two approaches to characterize the protection effect of PVP coating on the vNW-ssMNs. (f–i) SEM images of the surface morphologies of the PvNW-ssMNs and non-PVP-protected vNW-ssMNs after skin insertion: (f) annealed PvNW-ssMNs, (g) annealed vNW-ssMNs, (h) rinsed PvNW-ssMNs, and (i) rinsed vNW-ssMNs.

verify the MNs' penetration into skin, the blank ssMNs were stained with red fluorescence, rhodamine B, and then pressed against the pigskin, as shown in Figure 3b. After the removal of the ssMNs, an array of red fluorescence was retained in the pigskin, indicating a successful microneedle penetration. The resulting optical and fluorescence morphologies of both top and sectional views of the transdermal zone on pigskin are presented in Figure 3c,d, respectively, which shows evident penetrating holes. The observed maximum penetrating depth is about 300 μm, which is shorter than the length of the tips of ssMNs (~680 μm). It could be attributed the elastic shrinkage of pigskin that prevented complete insertion of the tips or led to the contraction of the bottom of the tip-holes. Nevertheless, the average 200–300 μm penetrating depth of the MN tips is enough to puncture the whole stratum corneum (10–15 μm) and epidermis (50–100 μm) layer and reach the dermis, ensuring the functionalization of the PvNW-ssMNs.

To investigate the integrity of vertical ZnO NWs after skin penetration, the morphology of the ZnO vertical NWs should be examined with microscopies. The OM or FM did not provide sufficient resolution to observe sub-microscale ZnO NWs. Instead, SEM was employed, but it required separation of MNs from the tissue to allow imaging of the MNs surface. Therefore, the MNs were separated from the tissue by two approaches, as illustrated in Figure 3e. In the first method, the skin tissue was completely burnt up at high temperature (800 °C for 30 min), whereas the metal MNs as well as the inorganic ZnO NWs were preserved at this temperature. The exposed MNs surface after skin removal was examined with SEM. The results shown in Figure 3f reveal that the PvNW-MNs were completely exposed after the skin was burnt up, whereas the ZnO NWs were still vertically presented on the MNs surface. In contrast, vertical ZnO NWs on vNW-MNs without PVP protection were rarely observed after skin removal, see Figure 3g, suggesting that the

DOI: 10.1021/acsami.8b18981
ACS Appl. Mater. Interfaces 2019, 11, 4809–4819

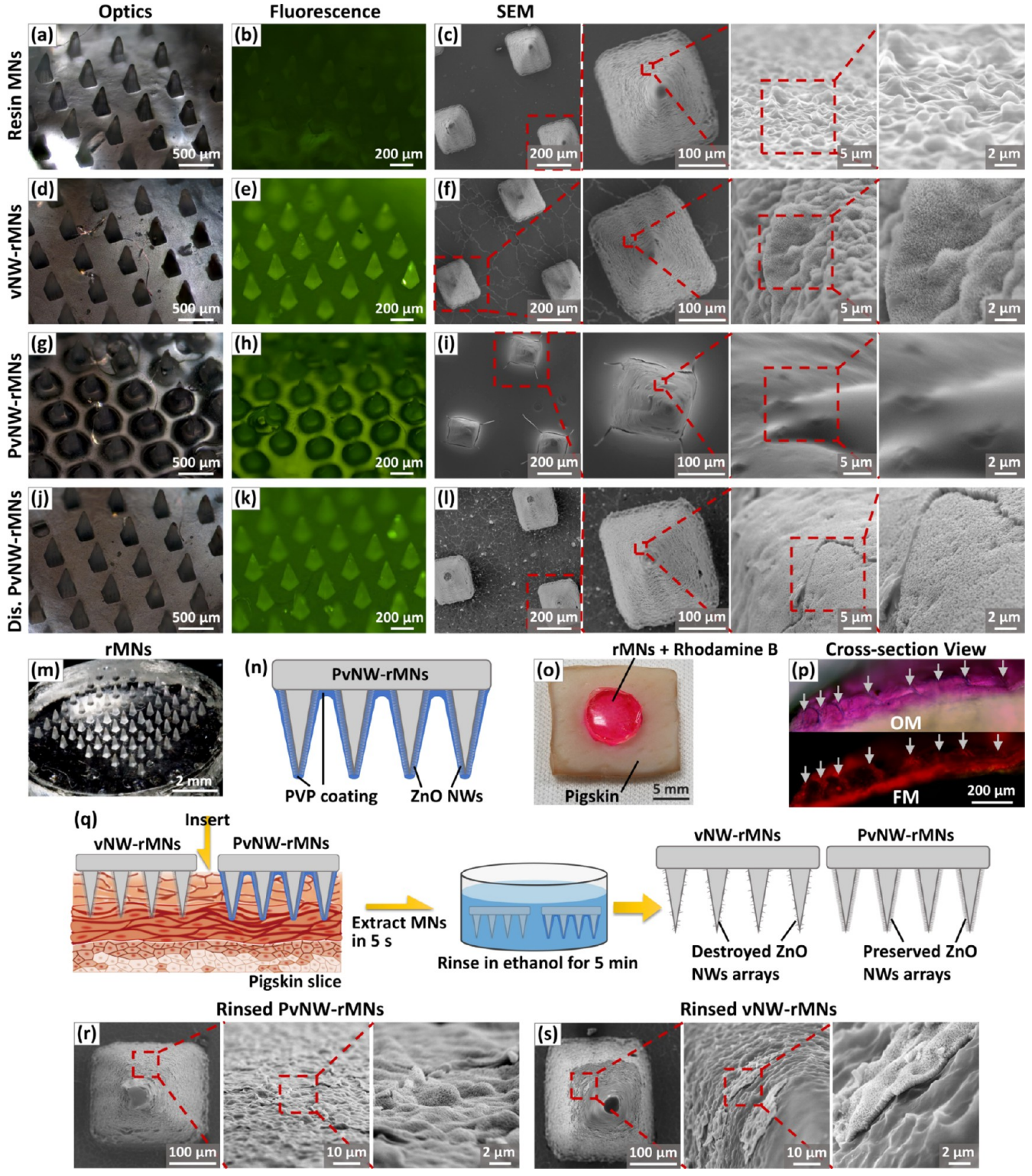

Figure 4. Characterization of nanostructures and the coating on resin MNs. Microscopic images of (a–c) the as-fabricated rMNs, (d–f) vertical ZnO NWs grown on rMNs, (g–i) PVP spray-coated vNW-rMNs, and (j–l) PvNW-rMNs with PVP coating dissolved. Microscopic images from left to right in each panel: optical microscopy, fluorescence microscopy, and SEM images at four magnifications, respectively. Protective effect of PVP coating on vNW-rMNs during the transdermal process. (m) Photographic image and (n) schematic of the structure of the PvNW-rMNs. (o) Photographic image of the rhodamine B stained rMNs insertion into the pigskin. (p) OM and FM images indicating the penetration of stained rMNs into the pigskin tissue (cross-sectional view). Arrows indicated the rMNs insertion sites. (q) Schematics of the approach to characterize the protection effect of PVP coating on the vNW-rMNs. (r, s) SEM images of surface morphologies of the PvNW-rMNs and non-PVP-protected vNW-ssMNs after skin insertion: (r) rinsed PvNW-rMNs and (s) rinsed vNW-rMNs.

ZnO NWs were likely to be destructed and peeled off during the MNs insertion process.

As for the second method to separate MNs from the tissue, the PvNW-MNs were first inserted into the skin but withdrawn

DOI: 10.1021/acsami.8b18981
ACS Appl. Mater. Interfaces 2019, 11, 4809–4819

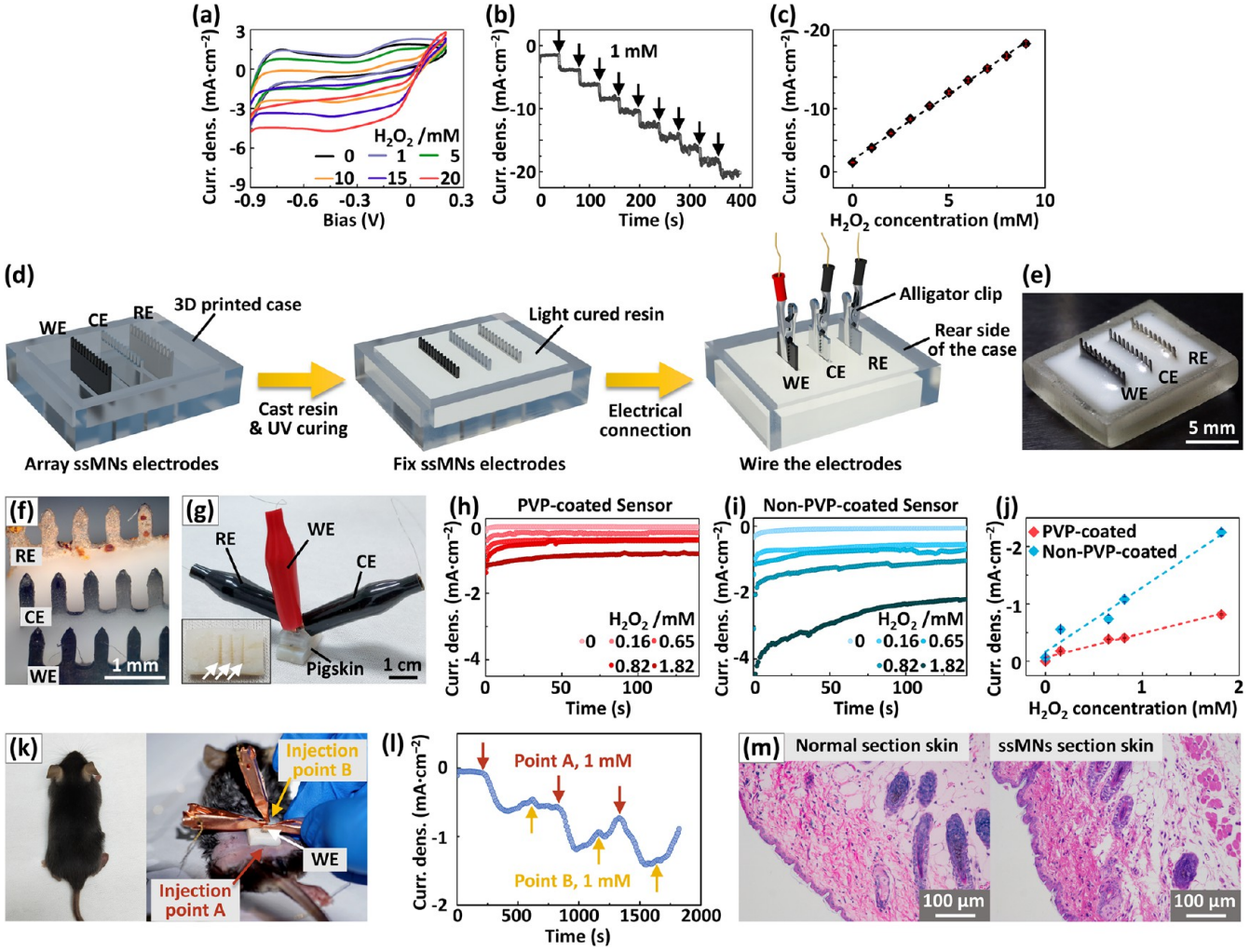

Figure 5. Ex vivo and in vivo electrochemical detection of H_2O_2 by PvNW-ssMNs sensors. (a) CV curves of Pt-sputtered vNW-ssMNs electrode to sense H_2O_2 solution with the concentrations of 0, 1, 5, 10, 15, and 20 mM. (b) Typical amperometric response of the Pt-sputtered vNW-ssMNs electrode to sense H_2O_2 solution upon the successive addition H_2O_2 concentration at the applied bias = −0.5 V. (c) Steady-state electrochemical currents upon different H_2O_2 concentrations. Data points were linearly fitted. (d) Schematic showing the integration process of the PvNW-ssMNs sensor. The Pt-sputtered vNW-ssMNs with an external PVP coating acted as the working electrode. (e) The photograph and (f) optical micrograph of the device. (g) Ex vivo measurement on pigskin soaked in H_2O_2 solution using the PvNW-ssMNs sensor. The inset shows the indentation on skin surface by the sensor. (h, i) Respective amperometric responses of PVP-coated and non-PVP-coated sensors applied on pigskins soaked in various H_2O_2 solutions. Bias = −1 V. (j) Steady-state amperometric responses (t > 100 s) were analyzed, and relations with H_2O_2 concentration were linearly fitted. (k) PvNW-ssMNs sensor was applied on a B6 mouse for in vivo experiments. The red and yellow arrows mark the subcutaneous injection points of the H_2O_2 solution. (l) Amperometric response of the PvNW-ssMNs sensor upon H_2O_2 injection at two injection positions. Bias = −1 V. Red and yellow arrows indicate the time points of injections. (m) Normal and ssMNs-treated mouse skin tissue stained with H&E for assessing skin irritation. The small navy blue spots indicate inflammatory cells distributed in the epidermis.

immediately (<5 s) so that the PVP was rarely dissolved in the tissue in such a short time range. The remaining PVP might protect the superficial ZnO NWs during the MNs withdrawal process. The PVP layer was then dissolved in ethanol to expose the MNs surface. Changing the solvent from DI to ethanol was for a better removal of skin tissue residuals. This allowed the SEM imaging to examine whether the PVP protected the MNs surface feature after both penetration and withdrawal processes. Similar to the results of the first skin removal approach, vertical ZnO NWs in Figure 3h were observed to be arrayed on the surface of the PvNW-MNs sample as neatly as those in Figure 2l, indicating that the PVP successfully protected the vertical ZnO NWs when the MNs were inserted and removed from the skin. In Figure 3i, the vNW-MNs without PVP coating rarely retained the vertical ZnO NWs on their surface after withdrawal from the skin, likely due to the peeling off of ZnO NWs during the transdermal process.

Taken together, these two experiments in parallel confirmed that the PVP coating effectively shielded the superficial nanowire structures from the destructive compression and friction from skin tissue during the MNs mechanical insertion process.

Resin microneedles array was employed as another example to further evaluate whether the microneedle protection approach via PVP spray coating was applicable to different MNs materials. The resin microneedle array was fabricated via a molding-UV curing approach.[29,36] The mixture of resin trimethylolpropane ethoxylate triacrylate (TMPTA) and curing agent 2-hydroxy-2-methylpropiophenone by 20:1 v/v proportion was injected into multiple-cavities-shaped poly(dimethylsiloxane) MNs mold,

DOI: 10.1021/acsami.8b18981
ACS Appl. Mater. Interfaces 2019, 11, 4809−4819

afterward the centrifugation was applied to drive the resin precursor solution into the microcavities. The resin was photopolymerized under UV illumination, then demolded, and rinsed. The complete process flow chart is plotted in the Supporting Information Figure S3. Following the same procedures on ssMNs, vertical ZnO NWs were fabricated on the resin MNs surface (vNW-rMNs) via hydrothermal approach and then coated by PVP via spraying.

The surface morphologies of the vNW-rMNs at different fabrication steps were characterized with OM, FM, and SEM. Micrographs are listed in Figure 4. The diameter of each resin tip was ~200 μm, and the length was about 600 μm. The total of 81 tips were aligned in a 9 × 9 array of 0.25 cm^2. The high-magnification SEM image in Figure 4c manifests a corrugated surface with height fluctuation in micrometer scale. The hydrothermal growth produced vertical ZnO NWs conformally covering each resin tip, with ~100 nm in diameter and ~2 μm in length for each ZnO NW, see Figure 4f. The ZnO NWs exhibited a bright green fluorescence under the illumination of UV light (330−380 nm), as shown in Figure 4e, corresponding to the photoluminescence emission of ZnO. However, the cured TMPTA is also able to be excited by UV light and to emit faint green light as shown in Figure 4b, which was confirmed by fluorescence spectroscopic study (see Figure S4 in the Supporting Information). The PVP was then coated on the vNW-rMNs surface (PvNW-rMNs) via spraying method, completely covering each tip, leading to an enhancement of green fluorescence (Figure 4h) and a fluctuation submerged surface (Figure 4i). The PVP coating could be readily dissolved in DI water to expose the superficial ZnO NWs again, where the revealed ZnO NWs shown in Figure 4l were observed to be as intact as those prior to PVP coating (Figure 4f).

Similarly, to verify the penetrating capability, the blank rMNs were stained with rhodamine B and then pressed against the pigskin, as Figure 4o shows. After the removal of rMNs, the pigskin was sectioned along one row of the tip-holes and then observed at the cross section in optical and fluorescence microscopes. The micrographs in Figure 4p show that penetrating holes had depth between 100 and 200 μm, which is shorter than that of the holes created by ssMNs with similar tip length (600 vs 680 μm). It may be attributed to the pyramid-shaped tips of rMNs, rather than the sword-shape tips of ssMNs, whose pyramid tips have a smaller volume with the same bottom area, thus the hole depth can be subjected to suppression by elastic shrinkage of the pigskin. The penetrating depth of rMNs barely allows puncturing of the stratum corneum and epidermis; therefore, they were considered to be more suitable for drug delivery rather than biosensing, since elongating the tips or modifying the tip shape would lead to difficulties in fabrication or frailty of transdermal applications.

To examine the integrity of vertical ZnO NWs on the rMNs after skin penetration, PvNW-rMNs were inserted into the pigskin and withdrawn within 5 s. Similar to the experiment on ssMNs, due to a short time range of MNs presenting in the skin, the PVP was rarely dissolved so that it could protect the vertical ZnO NWs during the MNs withdrawal process. To expose the MNs surface for examination of the ZnO NW morphology, the PVP layer was then dissolved in ethanol with skin residuals rinsed away simultaneously. The procedures are sketched in Figure 4q. Results presented in Figure 4r reveal that vertical ZnO NWs are intactly presented on the MNs surface if protected by PVP, whereas rMNs without the PVP coating experienced the peeling off of a large area of NWs after withdrawal from the skin, as shown in Figure 4s. These results demonstrated the PVP successfully protected the vertical ZnO NWs on rMNs when they were inserted and removed from the skin. Note that the rMNs would not tolerate temperature higher than 200 °C, thus they were not attempted to be separated from the skin by the approach of skin burning.

To examine whether the PVP coating effectively preserves the functionality of actual sensor, the vNW-ssMNs based on conductive ssMNs were constructed as a working electrode in an electrochemical biosensor. Sensing of H_2O_2 was demonstrated as the example, since H_2O_2 is a widespread biomarker in human body that is involved in many important physiological processes such as inflammatory responses.[37−40] As illustrated in Figure 1, superficial vertical ZnO nanowires were grown on the ssMNs, followed with sputter coating of a Pt layer thinner than 20 nm on the ZnO NWs (Supporting Information, Figure S5g), which possessed superior catalyzing capability of decomposing H_2O_2 to general electrochemical signals.[41] It should be noted that the PvNW-ssMNs electrochemical sensor was not limited in sensing H_2O_2 only, as the sensing of other biomarkers could be readily achieved by different surface functionalizations. The in vitro H_2O_2 sensing in PBS solution was performed using the Pt-coated vNW-ssMNs electrode, coupled with a commercial counter electrode and a reference electrode. The cyclic voltammetry was used for sensing different concentrations of H_2O_2 solution ranging from 0 to 20 mM (Figure 5a), which are higher than the typical H_2O_2 levels in human body,[38,42] with the aim for achieving strong enough responsive signals to properly evaluate the electrochemical characteristics of the working electrode. Reduction peaks at −0.45 V were observed, indicating the successful detection of H_2O_2. Amperometric response upon the stepwise increase of H_2O_2 concentration (by 1 mM each step) was also tested under −0.5 V bias (Figure 5b). The rise in H_2O_2 concentration induced a rapid increase of current signal (negative sign). The steady-state current densities (curr. dens.) were in a linear relation with H_2O_2 concentration (Figure 5c), with a sensitivity of 2.07 $mA{\cdot}cm^{-2}{\cdot}mM^{-1}$ (R^2 = 0.99821), exhibiting an excellent sensitivity compared with the reported H_2O_2 electrochemical sensor,[14] which benefited from the ZnO NWs/Pt composite structures as sensing receptors.

To examine whether the PVP coating effectively preserved the sensor's performance, sensing of H_2O_2 ex vivo on pigskin tissue and in vivo on C57BL/6 (B6) mice were investigated. Water-soluble PVP coating was spray-coated on the MNs surface to protect the fragile nanostructures. The PvNW-MNs served as the working electrode and were integrated with a Pt-deposited ssMNs counter electrode and a Ag/AgCl ink painted ssMNs reference electrode to build the H_2O_2 electrochemical sensor (Figure 5d−f). The sensor was applied on pigskins containing different concentrations of H_2O_2 (0, 0.16, 0.65, 0.82, and 1.82 mM, determined by hydrogen peroxide assay kit, see the Supporting Information Note 6 and Figure S6 for details) by presoaking pigskins in H_2O_2 solution (Figure 5g). The sensor without PVP coating was employed for comparison. For both PVP- and non-PVP-coated sensors, recorded current densities at the bias of −1 V enhanced with increase of H_2O_2 concentration, whereas the PVP-coated sensor produced significantly higher current signals compared to the non-PVP-coated sensor (Figure 5h,i). Steady-state (at t > 100 s) current densities were averaged for quantitative comparison, and the relations between the average steady-state current densities and the H_2O_2 concentration plotted in Figure 5j show linear profiles. The sensitivity of the PVP-coated sensor was 1.12 $mA{\cdot}cm^{-2}{\cdot}mM^{-1}$, about 3-folds

DOI: 10.1021/acsami.8b18981
ACS Appl. Mater. Interfaces 2019, 11, 4809−4819

higher than that of the non-PVP-coated sensor whose sensitivity was 0.42 $mA{\cdot}cm^{-2}{\cdot}mM^{-1}$. The higher sensitivity is likely due to the fact that the PVP coating effectively protected the superficial nanostructures, which were the sensing modulus.

In vivo transdermal H_2O_2 biosensing via the sensor was performed on C57BL/6 mice. The back of the mouse was shaved and the sensor was pressed on its back with ssMNs tips inserted into the skin (Figure 5k). Fluctuation of the H_2O_2 level in vivo was induced by subcutaneous injection of H_2O_2 solution. The subcutaneous injections were given at two different injection points, one of which was close to the WE (point A, distance to WE ∼4 mm) and the other was adjacent to the RE (point B, distance to WE ∼9 mm), as indicated in Figure 5k. H_2O_2 solutions (0.3 mL, 1 mM) were alternately injected at either points A or B with 200−300 s internals between each injection (indicated by red or yellow arrow). The amperometric response was recorded with −1 V bias applied, plotted in Figure 5l. Two types of characteristic peaks associated with the injection at points A and B were observed on the current density−time curve. The injection at point A induced an increasing current density of 0.62 ± 0.05 $mA{\cdot}cm^{-2}$ within ∼200 s, whereas the injection at point B induced a slight current density increase of 0.062 ± 0.03 $mA{\cdot}cm^{-2}$ within ∼50 s (both signs in the negative). The signals were repeatable during 3 cycles of independent injections. The higher signal at point A was likely due to the presence of a higher local concentration of H_2O_2 adjacent to the WE, whereas the H_2O_2 at point B would experience more diffusion barrier and decomposition in body fluids before reaching to WE.

Furthermore, the biosafety of the PvNW-ssMNs sensor was assessed by histological examination of a possible skin irritation and inflammatory effects. The PvNW-ssMNs sensor was applied on the skin of a B6 mouse and then −1 V electric bias was applied for 2000 s. The sensor was then removed and the mouse was returned to the cage for another 12 h. The treated local skin tissue were dissected and prepared to stain with hematoxylin and eosin (H&E). Compared to the control tissue the without PvNW-ssMNs sensor treatment (Figure 5m), no significantly increased density of infiltrated inflammatory cells was observed, indicating that minimal skin irritation and inflammation were induced by the application of PvNW-ssMNs sensor. It can be attributed to the minimally invasive characteristic of MNs and excellent biocompatibility and biodegradability of PVP[43] and ZnO NWs.[44−46]

Recently, Jin et al. reported a transdermal H_2O_2 MNs biosensor integrated with reduced graphene oxide/Pt nanoparticles nanohybrid (Pt/rGO).[47] The Pt/rGO nanostructures were also protected by the PVP layer to avoid mechanical destruction. Different from Jin et al.'s recent work that focused on the development of a single particular type of MNs sensor, our current work focused on the more general methodology of using water-dissolvable polymer coating as the protection layer to prevent the destruction of superficial nanostructures on MNs when inserted into the skin. This protection technique was examined on both metal MNs patch and resin MNs in an array, demonstrating the feasibility of this coating methodology to be applied on different types of MNs. Moreover, the current work employed vertical ZnO nanowires as model nanostructures for evaluating the polymer protection effects. Compared to the randomly aligned (Pt/rGO), these superficial vertical nanowires would be more challenging to protect during skin insertion process, highlighting the PVP coating technique as a robust methodology to protect superficial nanostructures on MNs.

CONCLUSIONS

In this work, a unique methodology of utilizing dissolvable and biosafe PVP coating to protect the fragile superficial nanostructures on MNs was demonstrated. The polymer coating effectively prevents the superficial nanostructures from mechanical damage during MNs transdermal process, whereas the polymer coating could rapidly dissolve in the interstitial fluid to expose the MNs surface for sensing functionality. The results were verified via morphology study on both metallic and resin MNs decorated with ZnO NWs on the surface, which revealed that the polymer coating was crucial to protect the superficial ZnO NWs structures after MNs penetrated the skin. The ZnO NWs-decorated MNs were further integrated as an electrochemical biosensor, and their sensing functionality on H_2O_2 biomarker in skin tissue both ex vivo and in vivo could be preserved by using the PVP protective coating. This work provided a unique strategy to solve the long-lasting issue of mechanical damage of fragile functional nanostructures on MNs during transdermal process, acting as a water-soluble "package" for MNs sensors. Not limited to nanowires, various types of nanostructures such as nanoparticles, nano-spiky, and nanoporous structures integrated on the surface of MNs could also be protected by our polymer-coating techniques. This study would open new opportunity of integrating nanostructures on MNs as sensing components, which could potentially facilitate the development of highly sensitive or multifunctional biodevices for real-time biosensing.

ASSOCIATED CONTENT

Supporting Information

The Supporting Information is available free of charge on the ACS Publications website at DOI: 10.1021/acsami.8b18981.

Experimental methods; design of the ssMNs; contact angle analysis of ssMNs with/without vertical ZnO NWs; fabricating process of TMPTA rMNs; emissive spectrum of cured TMPTA resin with the activation of UV light; in vitro electrochemical analysis of vNW-MNs electrodes after reducing, plating, and RF sputtering to deposit Pt on the surface; and standard absorbance−H_2O_2 concentration curve for H_2O_2 concentration analyzed in treated pigskin slices (PDF)

AUTHOR INFORMATION

Corresponding Authors

*E-mail: taojunz123@163.com (J.T.).
*E-mail: xiexi27@mail.sysu.edu.cn (X.X.).

ORCID

Fanmao Liu: 0000-0001-7590-8062
Gen He: 0000-0003-1394-0053
Xi Xie: 0000-0001-7406-8444

Author Contributions

⊥F.L. and Z.L. contributed equally to this work.

Author Contributions

F.L., Z.L., Q.J., Q.W., C.Y., H.-J.C., D.-a.L., J.T., and X.X. designed the experiments, analyzed the data, and wrote the manuscript. F.L., Z.L., Q.J., Q.W., C.Y., and H.-J.C. performed the experiments. F.L., Z.L., Q.J., L.Z., and X.X. performed the statistical analyses of the data sets and aided in the preparation of the display of communicating data sets. F.L., W.X., J.T., and X.X. provided the conceptual advice. J.T. and X.X. supervised the

DOI: 10.1021/acsami.8b18981
ACS Appl. Mater. Interfaces 2019, 11, 4809−4819

study. All authors discussed the results and assisted in the preparation of the manuscript.

Notes

The authors declare no competing financial interest.

■ ACKNOWLEDGMENTS

This work is supported in part by the National Natural Science Foundation of China (Grant Nos. 61771498, 31530023, 81671379, and 51705543) to X.X., J.T., W.X., and T.H. The authors wish to thank the Youth 1000 Talents Program of China (76120-18821104) to X.X., Youth Teacher Training Program of Sun Yat-Sen University (18lgpy18, 18lgpy21) to H.-J.C. and T.H., Science and Technology Program of Guangzhou, China (Grant No. 201803010097) to X.X., and Guangdong Province Science and Technology Plan Foundation (Nos. 2016A020215056, 2017A020215085, and 2017B090917001) to W.X. and X.X.

■ REFERENCES

(1) Rhee, S. G. H_2O_2, a Necessary Evil for Cell Signaling. *Science* **2006**, *312*, 1882−1883.
(2) Ohshima, H.; Tatemichi, M.; Sawa, T. Chemical Basis of Inflammation-induced Carcinogenesis. *Arch. Biochem. Biophys.* **2003**, *417*, 3−11.
(3) Ventrelli, L.; Marsilio Strambini, L.; Barillaro, G. Microneedles for Transdermal Biosensing: Current Picture and Future Direction. *Adv. Healthcare Mater.* **2015**, *4*, 2606−2640.
(4) Eyler, C. E.; Wu, Q.; Yan, K.; MacSwords, J. M.; Chandler-Militello, D.; Misuraca, K. L.; Lathia, J. D.; Forrester, M. T.; Lee, J.; Stamler, J. S.; Goldman, S. A.; Bredel, M.; McLendon, R. E.; Sloan, A. E.; Hjelmeland, A. B.; Rich, J. N. Glioma Stem Cell Proliferation and Tumor Growth are Promoted by Nitric Oxide Synthase-2. *Cell* **2011**, *146*, 53−66.
(5) Fukumura, D.; Kashiwagi, S.; Jain, R. K. The Role of Nitric Oxide in Tumour Progression. *Nat. Rev. Cancer* **2006**, *6*, 521−534.
(6) Schultz, W. Predictive Reward Signal of Dopamine Neurons. *J. Neurophysiol.* **1998**, *80*, 1−27.
(7) Chua, B.; Desai, S. P.; Tierney, M. J.; Tamada, J. A.; Jina, A. N. Effect of Microneedles Shape on Skin Penetration and Minimally Invasive Continuous Glucose Monitoring in vivo. *Sens. Actuators, A* **2013**, *203*, 373−381.
(8) Jiang, S.; Cheng, R.; Wang, X.; Xue, T.; Liu, Y.; Nel, A.; Huang, Y.; Duan, X. Real-time Electrical Detection of Nitric Oxide in Biological Systems with Sub-Nanomolar Sensitivity. *Nat. Commun.* **2013**, *4*, No. 2225.
(9) Luka, G.; Ahmadi, A.; Najjaran, H.; Alocilja, E.; DeRosa, M.; Wolthers, K.; Malki, A.; Aziz, H.; Althani, A.; Hoorfar, M. Microfluidics Integrated Biosensors: A Leading Technology towards Lab-on-a-Chip and Sensing Applications. *Sensors* **2015**, *15*, 30011−30031.
(10) López-Lorente, A. I.; Simonet, B. M.; Valcárcel, M. Analytical Potential of Hybrid Nanoparticles. *Anal. Bioanal. Chem.* **2011**, *399*, 43−54.
(11) Zhou, J.-X.; Tang, L.-N.; Yang, F.; Liang, F.-X.; Wang, H.; Li, Y.-T.; Zhang, G.-J. MoS_2/Pt Nanocomposite-functionalized Microneedle for Real-Time Monitoring of Hydrogen Peroxide Release from Living Cells. *Analyst* **2017**, *142*, 4322−4329.
(12) Zhang, Y.; Zhang, Y.; Wang, H.; Yan, B.; Shen, G.; Yu, R. An Enzyme Immobilization Platform for Biosensor Designs of Direct Electrochemistry Using Flower-Like ZnO Crystals and Nano-sized Gold Particles. *J. Electroanal. Chem.* **2009**, *627*, 9−14.
(13) Wang, Z. L. Zinc Oxide Nanostructures: Growth, Properties and Applications. *J. Phys.: Condens. Matter* **2004**, *16*, R829.
(14) Zhang, Y.; Xiao, J.; Lv, Q.; Wang, L.; Dong, X.; Asif, M.; Ren, J.; He, W.; Sun, Y.; Xiao, F.; Wang, S. In Situ Electrochemical Sensing and Real-Time Monitoring Live Cells Based on Freestanding Nanohybrid Paper Electrode Assembled from 3D Functionalized Graphene Framework. *ACS Appl. Mater. Interfaces* **2017**, *9*, 38201−38210.
(15) Xie, H.; Li, Y.-T.; Lei, Y.-M.; Liu, Y.-L.; Xiao, M.-M.; Gao, C.; Pang, D.-W.; Huang, W.-H.; Zhang, Z.-Y.; Zhang, G.-J. Real-Time Monitoring of Nitric Oxide at Single-Cell Level with Porphyrin-Functionalized Graphene Field-Effect Transistor Biosensor. *Anal. Chem.* **2016**, *88*, 11115−11122.
(16) Howes, P. D.; Chandrawati, R.; Stevens, M. M. Colloidal Nanoparticles as Advanced Biological Sensors. *Science* **2014**, *346*, No. 1247390.
(17) Holzinger, M.; Le Goff, A.; Cosnier, S. Nanomaterials for Biosensing Applications: A Review. *Front. Chem.* **2014**, *2*, No. 63.
(18) Yogeswaran, U.; Chen, S.-M. A Review on the Electrochemical Sensors and Biosensors Composed of Nanowires as Sensing Material. *Sensors* **2008**, *8*, 290−313.
(19) Davies, I. R.; Zhang, X. Nitric Oxide Selective Electrodes. In *Methods in Enzymology*; Poole, R. K., Ed.; Academic Press: 2008; Vol. *436*, pp 63−95.
(20) Kim, Y.-C.; Park, J.-H.; Prausnitz, M. R. Microneedles for drug and vaccine delivery. *Adv. Drug Delivery Rev.* **2012**, *64*, 1547−1568.
(21) Cahill, E. M.; O'Cearbhaill, E. D. Toward Biofunctional Microneedles for Stimulus Responsive Drug Delivery. *Bioconjugate Chem.* **2015**, *26*, 1289−1296.
(22) Lee, H.; Song, C.; Baik, S.; Kim, D.; Hyeon, T.; Kim, D.-H. Device-assisted Transdermal Drug Delivery. *Adv. Drug Delivery Rev.* **2018**, *127*, 35−45.
(23) Yu, J.; Zhang, Y.; Ye, Y.; DiSanto, R.; Sun, W.; Ranson, D.; Ligler, F. S.; Buse, J. B.; Gu, Z. Microneedle-array Patches Loaded with Hypoxia-Sensitive Vesicles Provide Fast Glucose-Responsive Insulin Delivery. *Proc. Natl. Acad. Sci. U.S.A.* **2015**, *112*, 8260−8265.
(24) Tang, J.; Wang, J.; Huang, K.; Ye, Y.; Su, T.; Qiao, L.; Hensley, M. T.; Caranasos, T. G.; Zhang, J.; Gu, Z.; Cheng, K. Cardiac Cell−integrated Microneedle Patch for Treating Myocardial Infarction. *Sci. Adv.* **2018**, *4*, No. eaat9365.
(25) Ye, Y.; Yu, J.; Wang, C.; Nguyen, N.-Y.; Walker, G. M.; Buse, J. B.; Gu, Z. Microneedles Integrated with Pancreatic Cells and Synthetic Glucose-Signal Amplifiers for Smart Insulin Delivery. *Adv. Mater.* **2016**, *28*, 3115−3121.
(26) Windmiller, J. R.; Valdés-Ramírez, G.; Zhou, N.; Zhou, M.; Miller, P. R.; Jin, C.; Brozik, S. M.; Polsky, R.; Katz, E.; Narayan, R.; Wang, J. Bicomponent Microneedle Array Biosensor for Minimally-invasive Glutamate Monitoring. *Electroanalysis* **2011**, *23*, 2302−2309.
(27) El-Laboudi, A.; Oliver, N. S.; Cass, A.; Johnston, D. Use of Microneedle Array Devices for Continuous Glucose Monitoring: A Review. *Diabetes Technol. Ther.* **2013**, *15*, 101−115.
(28) Sullivan, S. P.; Koutsonanos, D. G.; del Pilar Martin, M.; Lee, J. W.; Zarnitsyn, V.; Choi, S.-O.; Murthy, N.; Compans, R. W.; Skountzou, I.; Prausnitz, M. R. Dissolving Polymer Microneedle Patches for Influenza Vaccination. *Nat. Med.* **2010**, *16*, 915−920.
(29) Xie, X.; Pascual, C.; Lieu, C.; Oh, S.; Wang, J.; Zou, B.; Xie, J.; Li, Z.; Xie, J.; Yeomans, D. C.; Wu, M. X.; Xie, X. S. Analgesic Microneedle Patch for Neuropathic Pain Therapy. *ACS Nano* **2017**, *11*, 395−406.
(30) Li, B.; Wang, J.; Yang, S. Y.; Zhou, C.; Wu, M. X. Sample-free Quantification of Blood Biomarkers via Laser-Treated Skin. *Biomaterials* **2015**, *59*, 30−38.
(31) Chang, H.; Zheng, M.; Yu, X.; Than, A.; Seeni, R. Z.; Kang, R.; Tian, J.; Khanh, D. P.; Liu, L.; Chen, P.; Xu, C. A Swellable Microneedle Patch to Rapidly Extract Skin Interstitial Fluid for Timely Metabolic Analysis. *Adv. Mater.* **2017**, *29*, No. 1702243.
(32) Vanheusden, K.; Warren, W. L.; Seager, C. H.; Tallant, D. R.; Voigt, J. A.; Gnade, B. E. Mechanisms Behind Green Photoluminescence in ZnO Phosphor Powders. *J. Appl. Phys.* **1996**, *79*, 7983−7990.
(33) Djurišić, A. B.; Leung, Y. H.; Tam, K. H.; Ding, L.; Ge, W. K.; Chen, H. Y.; Gwo, S. Green, Yellow, and Orange Defect Emission from ZnO Nanostructures: Influence of Excitation Wavelength. *Appl. Phys. Lett.* **2006**, *88*, No. 103107.
(34) Teodorescu, M.; Bercea, M. Poly(vinylpyrrolidone) − A Versatile Polymer for Biomedical and Beyond Medical Applications. *Polym.-Plast. Technol. Eng.* **2015**, *54*, 923−943.

DOI: 10.1021/acsami.8b18981
ACS Appl. Mater. Interfaces 2019, 11, 4809−4819

(35) Tachikawa, S.; Noguchi, A.; Tsuge, T.; Hara, M.; Odawara, O.; Wada, H. Optical Properties of ZnO Nanoparticles Capped with Polymers. *Materials* **2011**, *4*, 1132−1143.
(36) Chen, H.-J.; Lin, D.-a.; Liu, F.; Zhou, L.; Liu, D.; Lin, Z.; Yang, C.; Jin, Q.; Hang, T.; He, G.; Xie, X. Transdermal Delivery of Living and Biofunctional Probiotics through Dissolvable Microneedle Patches. *ACS Appl. Bio Mater.* **2018**, *1*, 374−381.
(37) Varma, S. D.; Devamanoharan, P. S. Hydrogen Peroxide in Human Blood. *Free Radical Res. Commun.* **1991**, *14*, 125−131.
(38) Halliwell, B.; Clement, M. V.; Long, L. H. Hydrogen Peroxide in the Human Body. *FEBS Lett.* **2000**, *486*, 10−13.
(39) Wittmann, C.; Chockley, P.; Singh, S. K.; Pase, L.; Lieschke, G. J.; Grabher, C. Hydrogen Peroxide in Inflammation: Messenger, Guide, and Assassin. *Adv. Hematol.* **2012**, *2012*, No. 541471.
(40) Lennicke, C.; Rahn, J.; Lichtenfels, R.; Wessjohann, L. A.; Seliger, B. Hydrogen Peroxide − Production, Fate and Role in Redox Signaling of Tumor Cells. *Cell Commun. Signaling* **2015**, *13*, No. 39.
(41) Katsounaros, I.; Schneider, W. B.; Meier, J. C.; Benedikt, U.; Biedermann, P. U.; Auer, A. A.; Mayrhofer, K. J. J. Hydrogen Peroxide Electrochemistry on Platinum: Towards Understanding the Oxygen Reduction Reaction Mechanism. *Phys. Chem. Chem. Phys.* **2012**, *14*, 7384−7391.
(42) Forman, H. J.; Bernardo, A.; Davies, K. J. A. What is the Concentration of Hydrogen Peroxide in Blood and Plasma? *Arch. Biochem. Biophys.* **2016**, *603*, 48−53.
(43) Roy, N.; Saha, N.; Kitano, T.; Saha, P. Novel Hydrogels of PVP−CMC and Their Swelling Effect on Viscoelastic Properties. *J. Appl. Polym. Sci.* **2010**, *117*, 1703−1710.
(44) Gopikrishnan, R.; Zhang, K.; Ravichandran, P.; Baluchamy, S.; Ramesh, V.; Biradar, S.; Ramesh, P.; Pradhan, J.; Hall, J. C.; Pradhan, A. K.; Ramesh, G. T. Synthesis, Characterization and Biocompatibility Studies of Zinc Oxide (ZnO) Nanorods for Biomedical Application. *Nano-Micro Lett.* **2010**, *2*, 31−36.
(45) Li, Z.; Yang, R.; Yu, M.; Bai, F.; Li, C.; Wang, Z. L. Cellular Level Biocompatibility and Biosafety of ZnO Nanowires. *J. Phys. Chem. C* **2008**, *112*, 20114−20117.
(46) Zhang, Y.; Nayak, T. R.; Hong, H.; Cai, W. Biomedical Applications of Zinc Oxide Nanomaterials. *Curr. Mol. Med.* **2013**, *13*, 1633−1645.
(47) Jin, Q.; Chen, H.-J.; Li, X.; Huang, X.; Wu, Q.; He, G.; Hang, T.; Yang, C.; Jiang, Z.; Li, E.; Zhang, A.; Lin, Z.; Liu, F.; Xie, X. Reduced Graphene Oxide Nanohybrid−assembled Microneedles as Minimally-invasive Electrodes for Real-time Transdermal Biosensing. *Small* **2019**, No. 1804298.

NOTE ADDED AFTER ASAP PUBLICATION

Due to a production error, this paper was published on the Web on January 24, 2019, with the term "H_2O_2" incorrectly identified as "He_2O_2" in the Abstract. The corrected version was reposted on January 28, 2019.

DOI: 10.1021/acsami.8b18981
ACS Appl. Mater. Interfaces 2019, 11, 4809−4819